Asian Journal of Chemistry; Vol. 31, No. 2 (2019), 309-316

ASIAN JOURNAL OF CHEMISTRY

https://doi.org/10.14233/ajchem.2019.21581

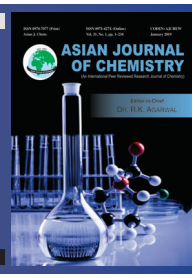

Hydrothermal Synthesis of Oxide and Carbonate Powders of (1-x)($Na_{0.5}Bi_{0.5}$)$TiO_{3-x}BaTiO_3$ Ceramics

M. Mesrar[1], T. Lamcharfi[1], N.S. Echatoui[1], F. Abdi[1] and F.Z. Ahjyaje[2]

[1]Signals, Systems and Components Laboratory (LSSC), Université Sidi Mohamed Ben Abdellah, Faculté des Sciences et Techniques de Fès, Imouzzer Road, B.P. 2202, Fes, Morocco
[2]Laboratory of Materials, Natural Substances, Environment and Modeling, Polydisciplinary Faculty of Taza, Université Sidi Mohamed Ben Abdellah, Imouzzer Road, B.P. 2202, Fes, Morocco

*Corresponding author: E-mail: nor-said.echatoui@usmba.ac.ma

Received: 13 July 2018; *Accepted*: 14 September 2018; *Published online*: 31 December 2018; AJC-19200

In this study, the synthesis of ferroelectric (1-x)($Na_{0.5}Bi_{0.5}$)$TiO_{3-x}BaTiO_3$ ceramics have been successfully prepared *via* a hydrothermal process, using bismuth oxide and barium carbonate. The characterization is done using X-ray diffraction, scanning electron microscope, Raman spectroscopy and dielectric measurements. The XRD patterns recorded at room temperature confirmed the formation of a single phase with rhombohedral structure. There is a transformation in crystal structure from rhombohedral to coexistence of rhombohedral and tetragonal to a single tetragonal phase with the increase in $BaTiO_3$ concentration in basic (1-x)($Na_{0.5}Bi_{0.5}$)TiO_{3-x}-$BaTiO_3$ composition. From SEM microscopy, the particle sizes are estimated in the range of 5-24 µm. The analysis of both Raman and the spectral deconvolution data of our samples also indicated the distortion of (1-x)($Na_{0.5}Bi_{0.5}$)$TiO_{3-x}BaTiO_3$ lattice with the addition of Ba^{2+} ion. Rietveld refinement method allows us to verify the morphotropic phase boundary at x = 0.05-0.07. The dielectric properties of the solid solution increase with a rise in Ba-TiO_3 content and shows optimum value at x = 0.07 owing to the co-existence of two ferroelectric phases. Based on these results, it is proved that morphotropic phase boundary in the studied system is included in the composition x = 0.05 and 0.07.

Keywords: ($Na_{0.5}Bi_{0.5}$)TiO_3, Hydrothermal method, Reitveld refinement, Raman spectroscopy, Dielectric measurements.

INTRODUCTION

Ferroelectric perovskites materials based on ($Na_{0,5}Bi_{0,5}$)-TiO_3 (NBT) are considered among the most promising candidate to replace zirconate titanate (PZT), which are widely used in electronic technology. However, lead oxides are toxic and volatile during heat processing, so these effects limit their uses in future devices. Hence, we observed strong demand for the use of lead-free materials in terms of environmental impact with properties comparable to their lead based counterparts.

Sodium bismuth titanate (NBT), first reported and studied by Smolenski *et al*. [1] and Jaffe *et al*. [2] considered to be an excellent candidate for lead-free ceramic materials because of piezoelectric and ferroelectric properties [3,4]. Sodium bismuth titanate shows strong ferroelectric properties of a large remanent polarization value P_r = 38 ºC/cm^2 [5] and has a high Curie temperature (T_c) = 320 ºC corresponds to a diffused phase transition and a phase transition point from ferroelectric to antiferroelectric (T_d) = 210 ºC [6,7], a large coercive field (73 kV/cm) and the high conductivity remain the major inconvenient for undoped NBT results in a low piezoelectric property, which then directed the investigation of NBT toward NBT-based solid solutions. One of the most important features of NBT is that it forms a morphotropic phase boundary with other perovskites possessing tetragonal symmetry, such as $K_{0.5}Bi_{0.5}TiO_3$ and $BaTiO_3$ leading to compositions that exhibit promising piezoelectric properties.

Sodium bismuth titanate ceramic has been conventionally prepared by solid-state method, yielding often large grains which are difficult to disperse and affect the sintering properties of sodium bismuth titanate, which reduces the possibilities of implementation in the devices [8,9]. Furthermore, it is well known that physical performances and surface properties are related to the particle shape and grain size. Recently, alternate methods of powder synthesis such as sol-gel synthesis [10], stearic acid gel method [11], emulsion method and citrate method [12] have been developed by several researchers. However, less investigation on (1-x)($Na_{0.5}Bi_{0.5}$)$TiO_{3-x}BaTiO_3$

(NBT·xBT) powders has been done by hydrothermal synthesis in last years.

Zhou *et al*. [4] obtained NBT powder in the temperature at 200 ºC under auto-generated pressure for 24 h. Moreover, several researchers proposed that NBT crystallizes in a higher NaOH concentrations and through a heating mechanism under low temperature. Accordingly, the hydrothermal synthesis of NBT-xBT powder was performed from simple precursors such as Bi_2O_3,TiO_2, $BaCO_3$ and Na_2CO_3 at 180 ºC under highly basic conditions. On the basis of the promising results of previous studies, we used hydrothermal method with the aim to prepare particles of a homogeneous size, in order to compare the microstructure properties with those prepared in the solid state.

EXPERIMENTAL

$(1-x)(Na_{0.5}Bi_{0.5})TiO_{3-x}BaTiO_3$ (NBT-xBT) ceramic was prepared by hydrothermal method. For this synthesis, we have used oxides (Bi_2O_3, TiO_2) of high purity (99.96 %; AppliChem GmbH, Ottoweg, Darmstadt, Germany) and carbonates ($BaCO_3$, Na_2CO_3) (99.96 %; AppliChem GmbH, Ottoweg, Darmstadt, Germany) which are used as Ba and Na precursors, respectively. Sodium hydroxide (99 %; AppliChem GmbH, Ottoweg, Darmstadt, Germany) served as the source of sodium cations, while at the same time ensuring a strongly basic environment. Stoichiometric amounts of the precursors were weighed according to the general chemical equation and mixed with acetone. The mixture was then dried and deagglomerated using agate mortar in order to obtain the desired compositions NBT-xBT for (x = 0, 0.03, 0.05, 0.06, 0.07, 0.08 and 0.1). The pH was then adjusted to 10 by dropwise addition of 10 M NaOH aqueous solution. The mixture was then transferred to a Teflon autoclave (50 mL capacity) and kept at 180 ºC in a furnace for 24 h. Finally, the precipitate was collected, centrifuged and washed several times with distilled water until pH value of outflow reached 7 and then dried at 80 ºC for 24 h. The chemical reaction for this synthesis is given in equation:

$$Na_2CO_3 + Bi_2O_3 + 4TiO_2 \longrightarrow 4(Na_{0.5}Bi_{0.5})TiO_3 + CO_2\uparrow$$
$$+$$
$$BaCO_3 + TiO_2 \longrightarrow BaTiO_3 + CO_2\uparrow$$

$$[(1-x)/4]Na_2CO_2 + [(1-x)/4]\ Bi_2O_3 + xBaCO_3 + TiO_2 \longrightarrow (1-x)(Na_{0.5}Bi_{0.5})TiO_3\text{-}xBaTiO_3 + [(1+3x)/4]CO_2\uparrow$$

Hydrothermal process of NBT-xBT based ceramics is shown in **Scheme-I**:

The resultant powder was deagglomerated using agate mortar in the presence of a few drops polyvinyl alcohol (2 % PVA) (binder and plasticizer). The powders were pressed under uniaxial pressing so as to obtain pellets having a diameter of 12 mm and a thickness of about 1 mm, under a pressure of 6 tons/cm^2 for 3 min, then these pellets were sintered for 4 h at 1000 ºC. The crystal structure of products was analyzed using a power X-ray diffraction (XRD) with a (XPERT-PRO with CuKα radiation with λ = 1.5406 Å). Crystallite sizes, weight fractions, crystalline fractions and lattice constants were determined from Rietveld fitting of the diffraction data. Morphology of the products was observed using an scanning electronic microscope (SEM). Raman spectroscopy has been used as an effective technique to investigate the structural evolution in

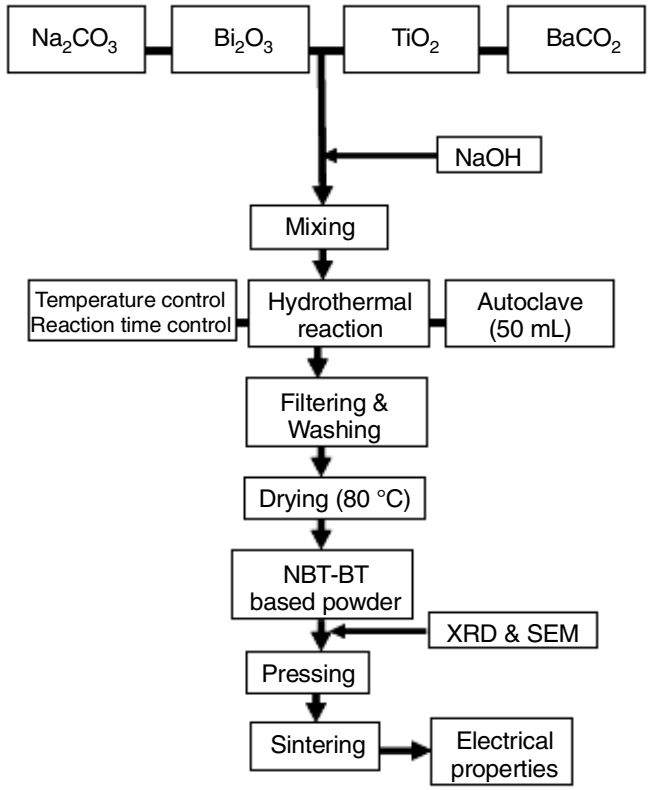

Scheme-I: Hydrothermal method process

ceramics. Temperature-dependent dielectric properties of the solid solutions were investigated using an Agilent impedance analyzer for different frequencies up to 1 MHZ and 600 ºC.

RESULTS AND DISCUSSION

XRD characterization of $(1-x)(Na_{0.5}Bi_{0.5})TiO_{3-x}BaTiO_3$ system: The hydrothermal reaction of NBT-xBT was carried out at 180 ºC for 24 h with at various barium concentration (*i.e*., x = 0, 0.03, 0.05, 0.06, 0.07, 0.08 and 0.1). The synthesized samples exhibited pure perovskite structure and no secondary phases were detected (Fig. 1a). The XRD peaks corresponding to NBT-xBT ceramic are relatively sharp, which suggest that the addition of $BaTiO_3$ increases the degree of crystallinity [13], implying that Ba^{2+} has successfully diffused into the NBT lattice to form a homogeneous solid solution NBT-xBT. From (Fig. 1a), it can be seen clearly that samples x = 0.05 and 0.07 crystallized predominantly in rhombohedral phase with small amount of tetragonal phase. Patterns from different compositions are quite similar, but reveal significant differences when zooming in peaks around 46º-47º (Fig. 1b). Obviously, the diffraction peaks of (200) shift to lower angles with increasing $BaTiO_3$ content, indicating the elongation of the unit cell of NBT-xBT system, which can be attributed to the high ionic radius of (rBa^{2+} = 1.61 Å) relative to (rNa^{+} = 1.39 Å) and (rBi^{3+} = 1.45 Å) lead to the expansion of the crystal lattice. Furthermore, this substitution creates the oxygen vacancies and brings about the lattice distortion [14].

Rietveld refinement analysis: Structural refinement was carried out for NBT-xBT ceramics with (x = 0.0, 0.03, 0.05, 0.06, 0.07, 0.08 and 0.1) using the Rietveld refinement method [15]. Fitted profiles of NBT-xBT were obtained using the Full-

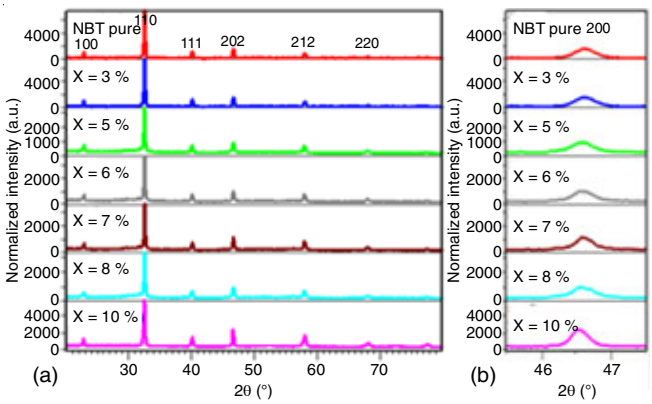

Fig. 1. X-ray diffraction pattern of NBT-xBT products hydrothermally synthesized at 180 °C for 24 h with NaOH concentration of 10 mol/L, with 2θ ranging (a) 10°-80° and (b) 46°-47°

TABLE-1
CALCULATED LATTICE PARAMETERS OF NBT-xBT CERAMICS BY REFINEMENT

X	Phase composition (%)	Lattice parameters			R (weighted profile) (%)
		a (Å)	b (Å)	c (Å)	
0	R3c 100	5.487	5.487	13.472	8.65
0.03	R3c 100	5.494	5.494	13.482	8.63
0.05	R3c 70.125	5.501	5.501	13.488	
	P4bm 29.875	5.498	5.498	3.900	8.26
0.06	R3c 68.267	5.514	5.514	13.552	
	P4bm 31.733	5.517	5.517	3.900	8.15
0.07	R3c 69.763	5.519	5.519	13.554	
	P4bm 30.237	5.515	5.515	3.901	7.32
0.08	P4bm 100	5.519	5.519	3.902	8.33
0.10	P4bm 100	5.522	5.522	3.894	8.73

prof software as shown in Fig. 2. The pseudo-Voigt function was used to define the peak profiles. It is observed that difference between various symmetries of spatial groups were tested by increasing compound (x) for NBT-xBT hydrothermal solutions. The profiles of XRD patterns experimentally observed and theoretically calculated display small difference as illustrated by a line blue ($Y_{Observed} - Y_{Calculated}$). The fitting parameters (R_{wp}, R_{exp}, R_w and σ) suggested that the refinement results are well-reliable. After repeated refinement, the R_{wp} values for all the samples are all less than 8.67 %. The unit-cell parameters of as-grown NBT crystal are a = b = 5.487 Å, c = 13.472 Å and $\alpha = \beta = 90°, \gamma = 120°$, which are similar to the data reported earlier [16,17]. Table-1 summarizes the lattice parameters and the fraction phase wt (%) in the two principal phases observed in present sample. Besides, we remarked that the limit of morphotropic phase remains unchangeable compared to the solid route [17]. Moreover, we mentiond that the fraction phase (quadratic phase P*4bm*) increases compared to the solid route (*i.e.* for x = 0.06 we found 29.913 wt % for the solid route and 31.733 wt % for hydrothermal route). The variations of lattice parameters are given in Table-1. With increasing $BaTiO_3$ content the tetragonality, (*i.e.* c/a) ratio decreased from 2.455 at x = 0 wt % to a minimum value of 2.453 at x = 5 wt % and then increases to 2.456 at x = 7 wt %. The results indicate that tetragonality c/a decreases gradually while the cell volume enlarges significantly. Moreover, the analysis of local structures around Bi, Na and Ba indicating that Bi-O and Na-O bond lengths are slightly shorter than those of Ba-O. This difference in bond lengths may explain the local distortion and the reduction of anisotropy of tetragonal crystal lattice indicated by the c/a ratio [18]. The insets of Fig. 2 show the corresponding model of rhombohedral and tetragonal structures. From structural refinement, all diffraction peaks of NBT-xBT ceramics confirmed

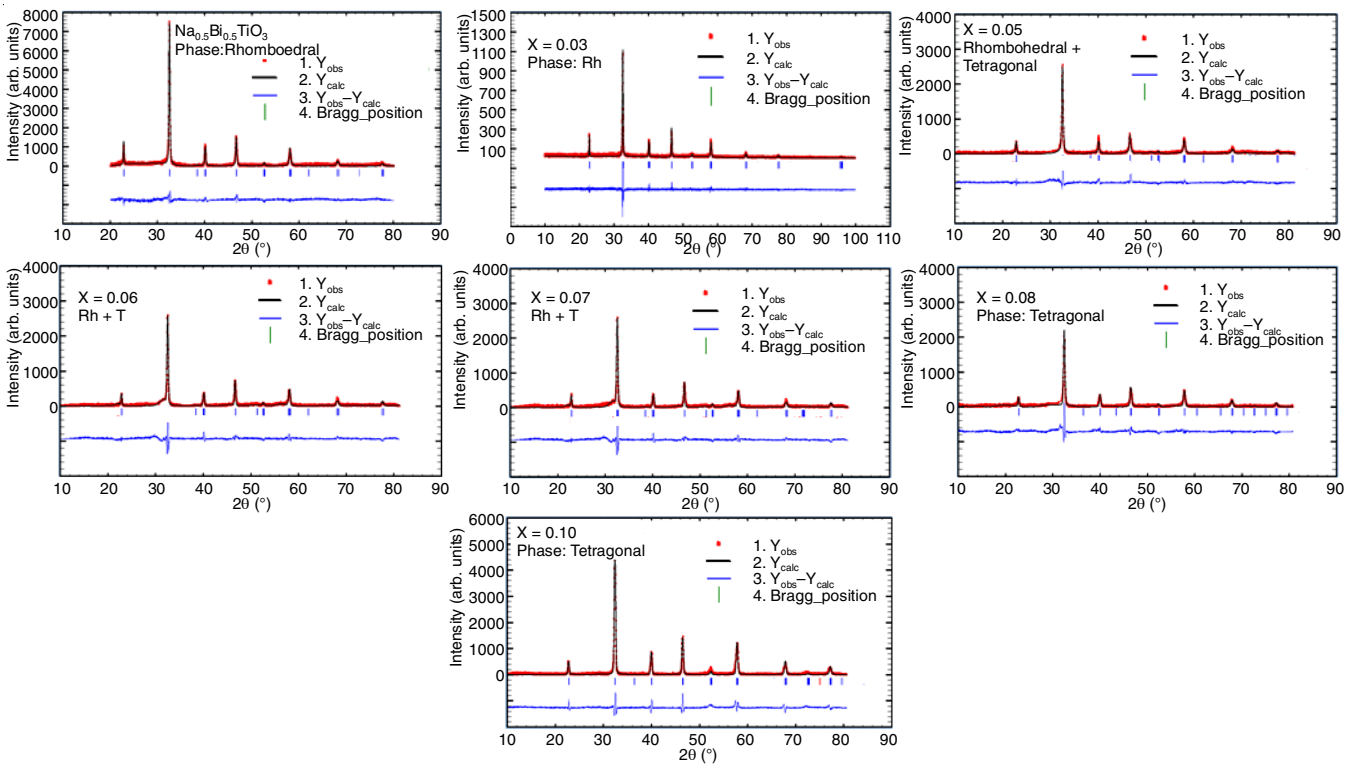

Fig. 2. Rietveld refinement for compounds NBT-xBT

that the compositions indexed to rhombohedral for x = 0.00, x = 0.03 with space group R*3c* and x = 0.08, x = 010 with space group P*4mm*. The refined profiles of these ceramics confirmed the successful formation of NBT-xBT phase during the synthesis process. The characteristics of phase structure transition were in good agreement with those reported in the literature [13,14, 17,19].

Raman analysis: Fig. 3 shows two distinct Raman spectra of NBT-xBT and $BaTiO_3$ recorded at room temperature in the wavenumber range of 1000-100 cm^{-1}. NBT displays three broad band′s centered at 136, 280 and 530 cm^{-1}, along with very weak bands at 866 cm^{-1}. On the other hand, the modes of $BaTiO_3$ are mainly centered at 350-200 cm^{-1} and 650-500 cm^{-1}. The group theory calculation made by Kreisel *et al*. [20], predicted 13 active modes, $\Gamma_{vib} = {}^4A_1 \pm 9E$ for the rhombohedral (R3c, $C^3{}_{V6}$, Z = 2) and the general irreducible representations of $BaTiO_3$ for tetragonal structure are as follows: $\Gamma_{vib} = {}^3F_{1u} + F_{2u}$, as per the group theory analysis. Thus, we can observed four modes in C_{4v} point group, which are $\Gamma_{C4v} = 3(A_1 + E) + E + B_1$ [21]. The mode at 136 cm^{-1} is assigned to A_1(TO1) mode symmetry, which is associated with Na-O vibration [13] and the broad band centered at 260 cm^{-1} is assigned to E(TO2) symmetry, which is dominated by Ti-O vibration [13]. The (TO3) mode centered at 650-520 cm^{-1} are associated with the vibration of TiO_6 octahedra [22]. The (TO3) latest mode (*i.e*. at 866 cm^{-1}) can be correlated to the presence of oxygen vacancies [22]. These modes are arranged into longitudinal (LO) and transverse (TO) components because of the electronic structure with polar character of lattice [23]. In addition, we found the same bands by the solid route, thus, similar changes of intensity and linewidth of the modes are found by the same route [17]. Simple examination of spectra shows clearly altered patterns between NBT pure and 10 % BT, a weakening and softening of mode near 136 cm^{-1}, shifting of mode near 280 cm^{-1} to the lower frequencies as composition (x) increases (up to about 264 cm^{-1} for x = 0.06) and moderate hardening of the modes near 570 cm^{-1} between 5 % and 8 % BT. Consequently, it can be easily seen that a drastic change occurs between 5 % and 7 % BT. These changes indicate a structural change in the unit cell. All of the above indicate a morphotropic phase boundary (MPB) between low $BaTiO_3$ concentrations 5 % BT and high $BaTiO_3$ concentrations 7 % BT, corresponding to rhombohedral and tetragonal phases found by XRD. Jones and Thomas [24] confirmed the existence of morphotropic transformation phase (MPB) around x = 0.05, which is in good agreement with present results. The deconvolution of spectrum of pure NBT with peakfit software using Gauss and Lorentzian area function, present nine vibration modes as shown Fig. 4. These results are in good agreement with those reported by Petzelt *et al*. [25] and Wang *et al*. [26]. When Ba^{2+} is added in the NBT structure, remarkable modifications are mentioned in the Raman spectra. The overall evolution of position frequency and full width at half maximum (FWHM) of individual peaks are plotted in Fig. 5. (i) For first mode (*i.e*. at 136 cm^{-1}) displays a shift to the higher frequencies as the composition (x) increases (up to about 141.5 cm^{-1} for x = 0.07); (ii) The broad band centered around 280 cm^{-1} is split into three modes (*i.e*. at 251, 286 and 320 cm^{-1}), this is also true for all samples, the last mode at 320 cm^{-1} E(TO3 + LO2) is a characteristic peak of the tetragonal symmetry of $BaTiO_3$ in Raman spectra. The intensity of this peak has not only increased but also shifted to the lower wavenumbers and this is well observed from the composition of x = 0.05. Furthermore, the FWHM shows an anomaly at x = 0.06 and presents a minimum with a further increase in composition (x); and (iii) The overlapping bands at 620-480 cm^{-1} are splitted into four modes (*i.e*. at 494, 530, 570 and 605 cm^{-1}) and presents two relatively prominent peaks (*i.e*. at 530 and 570 cm^{-1}). Moreover, this mode present a shift to the low frequencies as the composition (x) increases (upto about 564 cm^{-1} for x = 0.07). Furthermore, the FWHM shows an anomaly at x = 0.07 and presents a maximum with a further increase in composition (x).

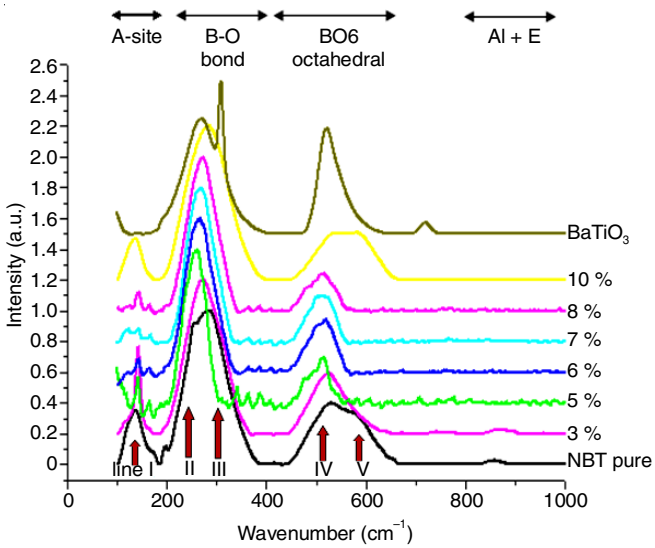

Fig. 3. Raman spectra of NBT-xBT for (x = 0.0, 0.03, 0.05, 0.065, 0.07, 0.08 and 0.1)

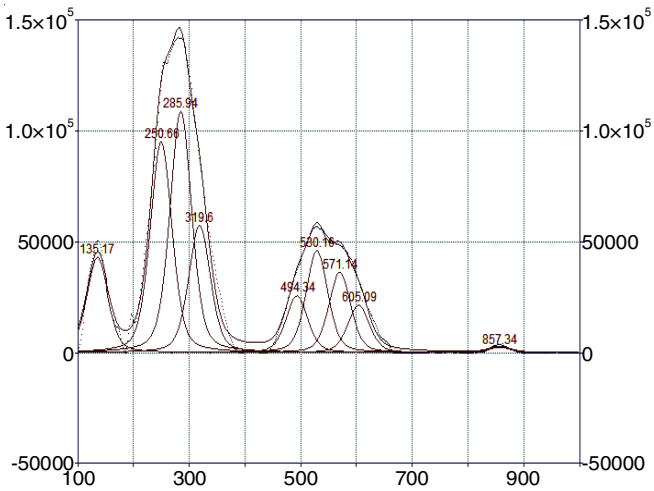

Fig. 4. Fitting of Raman spectra of NBT ceramic

The features clearly demonstrate a change in the phonon behaviour in the compound NBT-xBT. Finally, we observed that the position and FWHM of all the modes show a similar type of anomaly at x = 0.07. On the basis of these considerations, it is possible to conclude that rhombohedral-tetragonal phase coexists at x = 0.05-0.07, which is also observed in the XRD results.

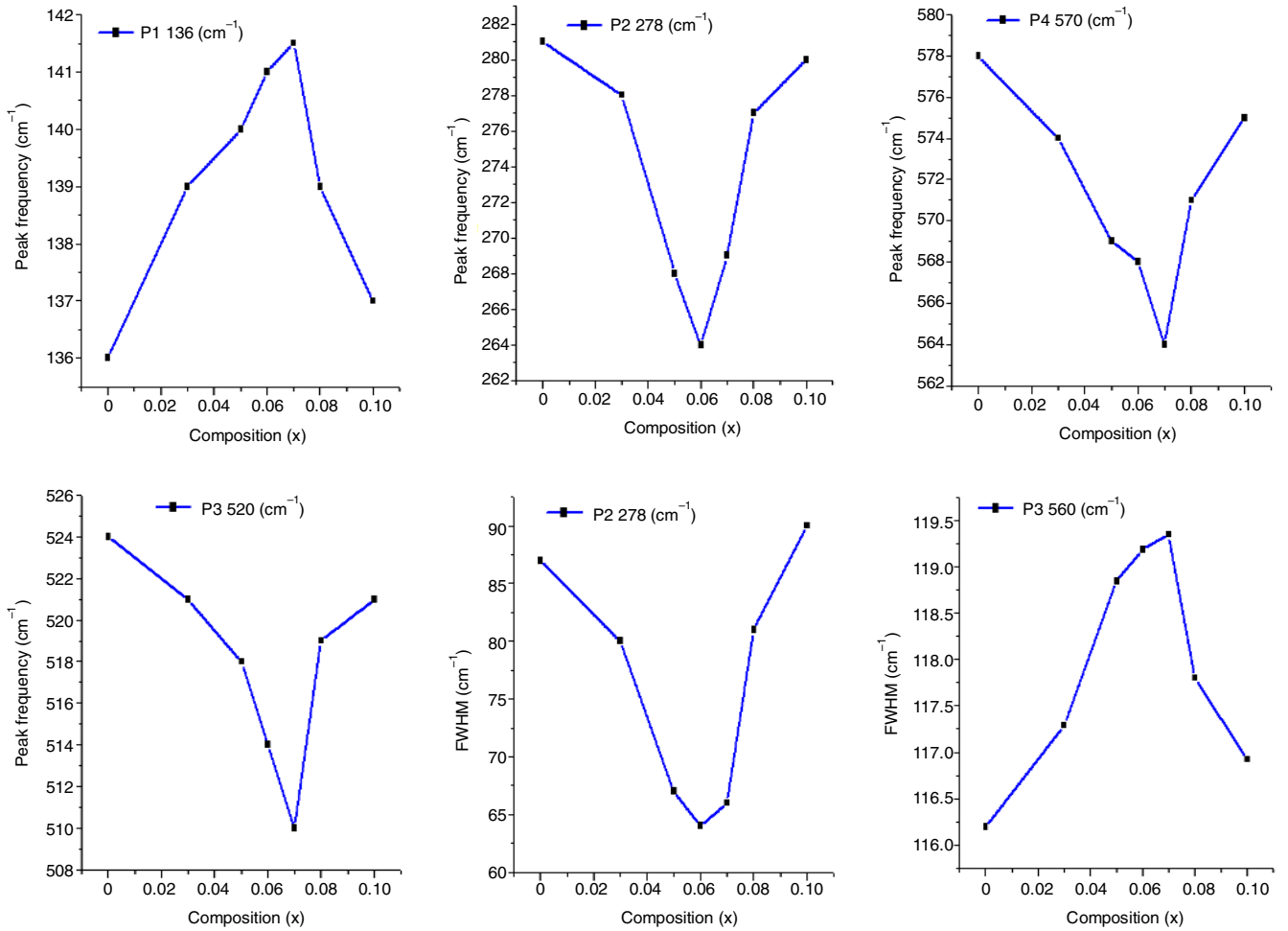

Fig. 5 Variations of peak positions (a) and (b) FWHM of different modes in the Raman spectra

Experimental density and micro-structural study: The SEM images of NBT-xBT (*i.e.* x = 0, 0.03, 0.05, 0.06, 0.07, 0.08 and 0.1) ceramics sintered at 1000 ºC, 4 h in air, is shown in Fig. 6. The microstructural details, grain size, morphology and grain boundaries can be observed from these micrographs. A small amount of pores is observed in the samples (x = 0.00 and 0.1) as well as all ceramics belonging into (x = 0.03, 0.05, 0.06, 0.07 and 0.08) are homogeneous and with a regular-shape. Experimental densities (ρex) of all the sintered NBT-xBT ceramic samples are also given in Table-2. Experimental densities (ρex) evolved proportionally with xBT content and it becomes maximum for x = 0.07. That enhancement of density can be related to the pores disparity in morphotropic phase boundary (MPB). However, slightly decreases at x = 0.1 depending on the porosity observed. The pure NBT ceramic has a microstructure with non-uniform grains of hexagonal aspect, while the addition of BT ceramic into NBT matrix promotes a change to homogeneous and hexagonal grains at MPB. Furthermore, the grain shape is changed to rectangular with higher BT content at x = 0.1. The significant changes in grain size can be easily observed (Fig. 7). The grains gradually grew when BT content is added, and it becomes maximum at x = 0.07. The average grain size increased brutally up to 24.26 μm then decrease to 5.53 μm at x = 0.1. This reduction may be due to the change of structure (Rh+T towards T) evoked in the XRD analysis and confirmed by the results given in the literature [17,19,27,28].

TABLE-2
MICRO STRUCTURAL PARAMETERS OF NBT-xBT CERAMICS

NBT-xBT	Average grain size (μm)	Exp. density (g/cm^3)
x = 0.00	11.27	5.960
x = 0.03	12.47	5.990
x = 0.05	20.99	6.013
x = 0.06	21.88	6.019
x = 0.07	24.26	6.025
x = 0.08	11.81	5.920
x = 0.10	5.53	5.910

Dielectric study: Fig. 8 shows the temperature dependence of ε_r (T) and tan δ at different frequencies (100, 200, 300 and 400 KHz) of NBT-xBT (x = 0.0, 0.03, 0.05, 0.06, 0.07, 0.08 and 0.1) ceramics. It is observed that ε_r increases monotonically on increasing temperature at all the frequency, which is a normal behaviour of polar dielectric materials. The variation of tan δ with temperature also follows the similar nature of variation as that of dielectric constant except at high temperatures (~ 400 ºC), it can be seen that there is an exponential-like increasing in tan δ curve towards of high values, generated by oxygen vacancies that form dipolar defects [29]. Further, our observed variations of dielectric constant with temperature at different frequencies are analogous with the reported using solid-state route [18-20]. Two major peaks are observed in all the NBT-xBT ceramics. The first peak in the 242-286 ºC regions corresponds to the depolarization temperature (T_d)

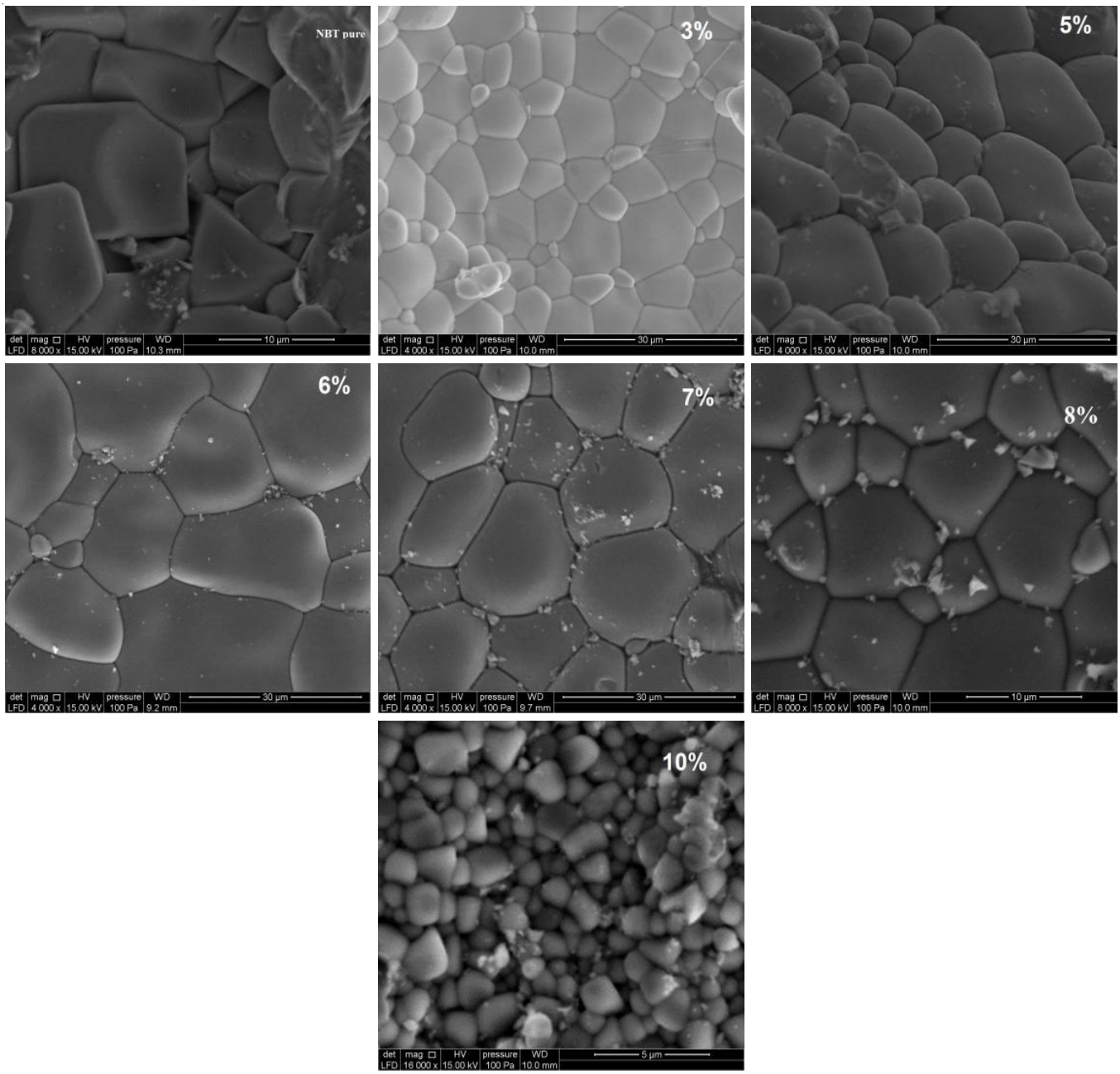

Fig. 6. Cross-section SEM images of NBT-xBT ceramics

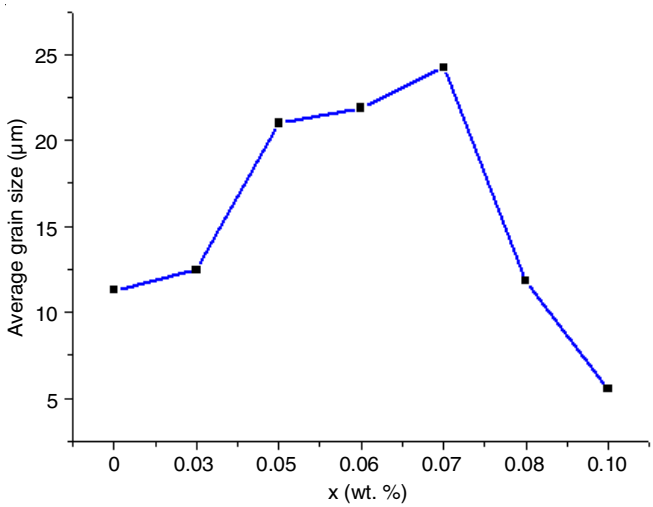

Fig. 7. Variation of grain size with x(wt.%) in BT

(Table-3), at this temperature the ferroelectric state undergoes to antiferroelectric state transition [30]. The second peak T_m (where ε_r reaches a maximum value) corresponds to the transition from antiferroelectric (non centrosymmetric space group: R*3c*) to paraelectric phase transition (non centrosymmetric space group: P*4mm*) transition that can be associated to structural transition from room temperature rhombohedral to tetragonal phase [29,30]. The value of dielectric constant of pure and doped NBT-xBT at x = 0.07 has been improved from 3979 to 10892 at T_m temperature (Table-3). Consequently, it can be concluded that effect of BT doping has significantly increased the value of dielectric constant near of MPB. Moreover, dielectric peaks at T_m for the ceramics are relatively broad and exhibited strong frequency dependence which is manifested by a diffuse character. Thus, it is evident that doping induces two major changes in the NBT system: (i) shifting of peak temperature (T_m) to lower

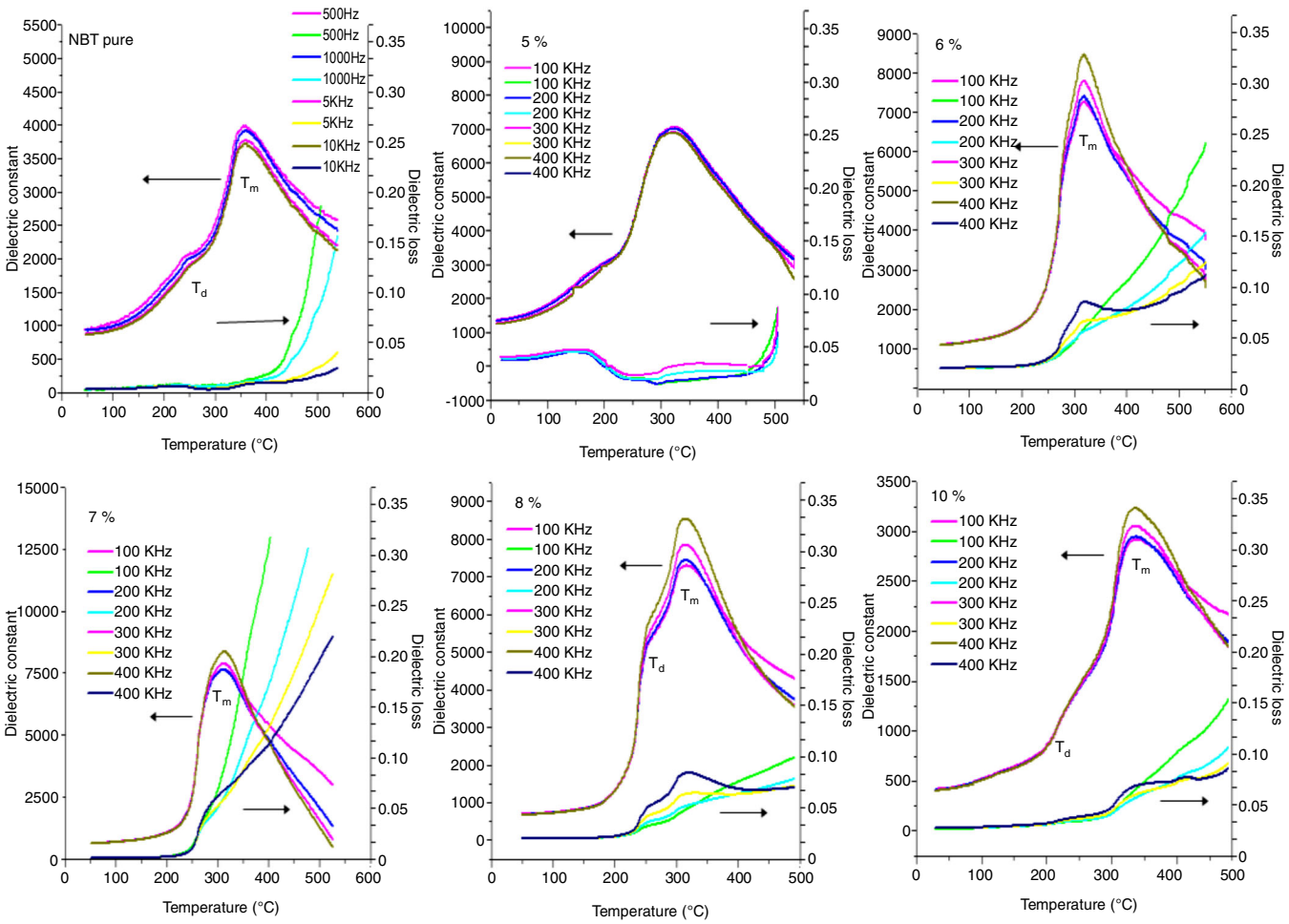

Fig. 8. Temperature-dependent dielectric constant and dielectric loss of NBT-xBT ceramics at 100, 200, 300 and 400 kHz from 25 to 600 °C

TABLE-3
DIELECTRIC PROPERTIES OF NBT-xBT CERAMICS AT 100 KHz FREQUENCY

BT content	ε_r at RT	tan δ at RT	T_d (°C)	T_m (°C)	ε_r at T_m
x = 0.00	962	0.015	242	357	3979
x = 0.05	1078	0.023	278	324	6788
x = 0.06	1023	0.018	286	306	6958
x = 0.07	1051	0.024	275	291	10892
x = 0.08	785	0.021	259	313	8308
x = 0.10	652	0.017	245	332	3259

temperature, and (ii) broadening of dielectric spectra. Lowering of transition temperature with $BaTiO_3$ concentration can be attributed to increase in isovalency of NBT-xBT solid solution at A-site by partial replacement of (Bi^{3+}/Na^+) by Ba^{2+} [30]. The dispersions in dielectric can also be explained by the strong heterogeneity induced at A-site due to the partial substitution of Bi^{3+} and Na^+ by Ba^{2+}, which perturbed the coulomb interaction at long range. These results are in good agreement with the work of Babu *et al.* [31] and Devi *et al.* [32].

Conclusion

(1-x)($Na_{0.5}Bi_{0.5}$)$TiO_{3-x}BaTiO_3$ (NBT-xBT) (x= 0.0, 0.03, 0.05, 0.06, 0.07, 0.08 and 0.1) ceramics were synthesized at 180°C using a hydrothermal method in the presence of 10 M NaOH. We utilized, furthermore, bismuth oxide and barium carbonate as initial precursors. X-ray diffraction study proves the formation of crystalline structure without any trace of the secondary phase. Moreover, Rietveld refinement method confirms the existence of MPB by the coexistence of rhombohedral and tetragonal peaks at x = 0.05-0.07. The results suggestted that the morphology of powders was significantly influenced by $BaTiO_3$ content in morphotropic phase boundary (MPB). In addition, the grains of ceramics with x = 0.07 are more homogeneous and the microstructure is more compact. The Raman spectra showed several predominant modes associated with A-site vibrations, TiO_6 octahedral vibrations and oxygen displacement. The modes in high-frequency range exhibited discontinuous changes across the rhombohedral-tetragonal transition while a lattice mode at 136 cm^{-1} is found to exhibit anomalies in its intensity and linewidth. Dielectric data as a function of temperature shows lower shift of dielectric transition temperature from 357 ºC to 291 ºC. Consequently, it is found that addition of $BaTiO_3$ plays a significant role in improving the dielectric properties of NBT-xBT ceramics near morphotropic phase boundary (MPB), where ε_r is maximum.

CONFLICT OF INTEREST

The authors declare that there is no conflict of interests regarding the publication of this article.

REFERENCES

1. G.A. Smolenski, V.A. Isupov, A.I. Agranovskaya and N.N. Krai-nik, *Soviet Physics-Solid State*, **2**, 2651 (1961).
2. B. Jaffe, W.R. Cook Jr. and H. Jaffe, eds.: J.P. Roberts and J.P. Popper, Piezoelectric Ceramics; In Non-Metallic Solids. A Series of Monographs, Academic Press: New York, vol. 3 (1971).
3. Q. Xu, S. Chen, W. Chen, S. Wu, J. Lee, J. Zhou, H. Sun and Y. Li, *Alloys Compd.*, **381**, 221 (2004); https://doi.org/10.1016/j.jallcom.2004.02.057.
4. X. Zhou, C. Jiang, H. Luo, C. Chen, K. Zhou and D. Zhang, *Ceram. Int.*, **42**, 18631 (2016); https://doi.org/10.1016/j.ceramint.2016.08.208.
5. K.S. Rao, K.C.V. Rajulu, B. Tilak and A. Swathi, *Nat. Sci.*, **2**, 357 (2010).
6. A. Sasaki, T. Chiba, Y. Mamiya and E. Otsuki, *Jpn. J. Appl. Phys.*, **38(no 9S)**, 5564 (1999); https://doi.org/10.1143/JJAP.38.5564.
7. K.-S. Yang, M.-J. Choi, J.-S. Choi, J.-H. Eom, B.-J. Park, S.-Y. Lee and S.-G. Yoon, *Sens. Actuators A: Phys.*, **243**, 117 (2016); https://doi.org/10.1016/j.sna.2016.03.018.
8. P. Pookmaneea, S. Phanichphanta, R. B. Heimann, *CFI-Ceram. Forum Int.*, **78**, E25 (2001).
9. M. Spreitzer, M. Valant and D. Suvorov, *J. Mater. Chem.*, **38**, 313 (2004).
10. M. Cernea, E. Andronescu, R. Radu, F. Fochi and C. Galassi, *J. Alloys Compd.*, **490**, 690 (2010); https://doi.org/10.1016/j.jallcom.2009.10.140.
11. J. Hao, X.H. Wang, R.Z. Chen and L. Li, *Mater. Chem. Phys.*, **90**, 282 (2005); https://doi.org/10.1016/j.matchemphys.2004.05.019.
12. B.H. Kim, S.J. Han, J.H. Kim, J.H. Lee, B.K. Ahn and Q. Xu, *Ceram. Int.*, **33**, 447 (2007); https://doi.org/10.1016/j.ceramint.2005.10.022.
13. H. Lidjici, B. Lagoun, M. Berrahal, M. Rguitti, M.A. Hen-tatti and H. Khemakhem, *J. Alloys Compd.*, **618**, 643 (2015); https://doi.org/10.1016/j.jallcom.2014.08.161.
14. H. Hu, M. Zhu, Y. Hou and H. Yan, *IEEE Trans. Ultrason. Ferroelectr. Freq. Control*, **56**, 897 (2009); https://doi.org/10.1109/TUFFC.2009.1121.
15. H.M. Rietveld, *J. Appl. Cryst.*, **2**, 65 (1969); https://doi.org/10.1107/S0021889869006558.
16. S. Sasikumar, R. Saravanan, S. Saravanakumar and K. Aravinth, *J. Mater. Sci.: Mater. Electron.*, **28**, 9950 (2017); https://doi.org/10.1007/s10854-017-6753-5.
17. M. Mesrar, T. Lamcharfi, N. Echatoui, F. Abdi and A. Harrach, *Asian J. Chem.*, **30**, 1012 (2018); https://doi.org/10.14233/ajchem.2018.21116.
18. H. Yabuta, H. Tanaka, T. Furuta, T. Watanabe, M. Kubota, T. Matsuda, T. Ifuku and Y. Yoneda, *Scient. Rep.*, **7**, 45842 (2017); https://doi.org/10.1038/srep45842.
19. Q. Xu, Z. Song, W. Tang, H. Hao, L. Zhang, M. Appiah, M. Cao, Z. Yao, Z. He and H. Liu, *J. Am. Ceram. Soc.*, **98**, 3119 (2015); https://doi.org/10.1111/jace.13693.
20. J. Kreisel, AM. Glazer, G. Jones, P.A. Thomas, L. Abello and G. Lucazeau, *J. Phys.: Condens. Matter.*, **12**, 3267 (2000); https://doi.org/10.1088/0953-8984/12/14/305.
21. D.P. Dutta, M. Roy, N. Maiti and A.K. Tyagi, *Phys. Chem. Chem. Phys.*, **18**, 9758 (2016); https://doi.org/10.1039/C5CP07736B.
22. J. Suchanicz, I. Jankowska-Sumara and T.V. Kruzina, *J. Electroceram.*, **27**, 45 (2011); https://doi.org/10.1007/s10832-011-9648-5.
23. B. Parija, T. Badapanda, P. Sahoo, M. Kar, P. Kumar and S. Panigrahi, *Proces. Appl. Ceram.*, **7**, 73 (2013); https://doi.org/10.2298/PAC1302073P.
24. G.O. Jones and P.A. Thomas, *Acta Crystallogr. B*, **58**, 168 (2002); https://doi.org/10.1107/S0108768101020845.
25. J. Petzelt, S. Kamba, J. Fábry, D. Noujni, V. Porokhonskyy, A. Pashkin, I. Franke, K. Roleder, J. Suchanicz, R. Klein and G.E. Kugel, *J. Phys. Condens. Matter*, **16**, 2719 (2004); https://doi.org/10.1088/0953-8984/16/15/022.
26. C. Wang, T. Xia, X. Lou and S. Tian, *J. Mater. Sci.*, **52**, 11337 (2017); https://doi.org/10.1007/s10853-017-1306-0.
27. L. Liu, Z. Yang, M. Wu, L. Fang and C. Hu, *J. Alloys Compd.*, **507**, 196 (2010); https://doi.org/10.1016/j.jallcom.2010.07.154.
28. S.R. Kanuru, K. Baskar and R. Dhanasekaran, *Ceram. Int.*, **42**, 6054 (2016); https://doi.org/10.1016/j.ceramint.2015.12.162.
29. S. Sayyed, S.A. Acharya, P. Kautkar and V. Sathe, *RSC Adv.*, **5**, 50644 (2015); https://doi.org/10.1039/C5RA05617A.
30. P. Jaita, A. Watcharapasorn and S. Jiansirisomboon, *Nano Res. Lett.*, **7**, 24 (2012); https://doi.org/10.1186/1556-276X-7-24.
31. J. Bubesh Babu, M. He, D.F. Zhang, X.L. Chen and R. Dhanasekaran, *Appl. Phys. Lett.*, **31**, 102901 (2007); https://doi.org/10.1063/1.2709917.
32. C. Sameera Devi, M. Buchi Suresh, G.S. Kumar and G. Prasad, *Mater. Sci. Eng. B*, **228**, 38 (2018); https://doi.org/10.1016/j.mseb.2017.11.005.